SSRG International Journal of Electrical and Electronics Engineering
ISSN: 2348-8379/ https://doi.org/10.14445/23488379/IJEEE-V13I10P108

Volume 13 Issue 10, 106-121, October 2026
© 2026 Seventh Sense Research Group®

Original Article

A Low-Cost Embedded System for Non-Technical Loss Detection in Low-Voltage Distribution Networks

Yordan Zosimo Cerron Armas[1], Cristhian Paolo Poma Mercado[2], Andy Quispe Mendoza[3], Jezzy James Huaman Rojas[4]

[1,2,3,4]*School of Electrical Engineering, Universidad Continental, Huancayo, Peru.*

[4]*Corresponding Author: jhuamanroj@continental.edu.pe*

Received: 09 July 2026 Revised: 25 September 2026 Accepted: 30 September 2026 Published: 28 October 2026

Abstract *- A low-cost wireless embedded system was developed and evaluated for the local and real-time detection of non-technical losses caused by electrical bypasses in low-voltage service drops. The architecture consists of two ESP32-based measurement nodes equipped with PZEM-004T V3 modules and interconnected through ESP-NOW. Node A measures the electrical variables at the service connection point, whereas Node B acquires the billing-point variables, processes the received telemetry, and displays the operating status through a local web dashboard. The detection model incorporates the estimated resistive loss of the service drop and applies a current-dependent dynamic threshold to distinguish technical losses from unexplained power discrepancies. Measurement pairs are validated through sequence identification, timestamp-based synchronization, and wireless-link quality criteria before classification. The experimental campaign comprised 40 scenarios, including 20 controlled tests and 20 different residential service drops with conductor cross-sectional areas of 6 and 10 mm², lengths from 4 to 25 m, and different load profiles. Thirty-eight acquisitions satisfied the established quality criteria. The system obtained 9 true positives, 28 true negatives, 0 false positives, and 1 false negative, corresponding to an accuracy of 97.37%, sensitivity of 90.00%, specificity of 100.00%, and precision of 100.00%. The ESP-NOW link achieved an overall packet error rate of 0.79% and a mean transmission latency of 4.36 ms. The results show that technical-loss compensation and acquisition-quality control reduce false alerts under the evaluated high-load, transient, and nonlinear operating conditions.*

Keywords *- Embedded systems, Electrical instrumentation, Non-Technical losses, Electricity theft detection, Low-Voltage electrical distribution networks.*

1. Introduction

Energy losses in distribution networks are divided into two categories: technical losses and Non-Technical Losses (NTLs). Once electricity is in the distribution network, technical losses are caused by the physical properties of electricity. An example of this is the heat produced in cables and transformers. NTLs comprise several types of energy fraud. Non-technical losses are attributed to energy consumed without being billed, electricity theft, tampering with the consumption meter, hidden connections, and administrative/metering errors. NTLs affect the revenues of the distribution company, increase financial losses, and worsen the quality of the electricity supplied. NTLs also have the potential to generate new costs for legitimate users [1, 2].

One of the most significant types of non-technical loss is the clandestine connection, which is carried out upstream of the commercial meter. This occurs when a load is connected to the distribution network before the point where energy is measured for billing purposes. Therefore, energy theft goes unnoticed, either totally or partially, by the customer's energy meter. It also limits the applicability of consumption-based techniques and the effectiveness of standard field inspections.

Many methods for identifying NTLs have been documented in the literature. Some methods are based on the presence of Advanced Metering Infrastructure (AMI) and use data collected by smart meters to analyze and identify irregular uses. Other methods involve the use of machine learning and deep learning, including hybrid techniques, to analyze electrical data together with network topology and classification data [2-7]. These approaches have contributed greatly to the progress of the area in networks with historical data, AMI, and centralized data availability. Their application may be limited to individual low-voltage connections, environments with low technological availability, or if the illegal connection is made before the commercial meter.

Consumption pattern-based methods require representative historical records and, in many cases, labeled datasets for training and validation [3-6]. Hybrid approaches may require topological information, distributed

This is an open access article under the CC BY-NC-ND license (http://creativecommons.org/licenses/by-nc-nd/4.0/)

measurements, or electrical models of the network [7]. These conditions are not always available in low-voltage areas due to insufficient infrastructure. Also, direct visual inspection may not be enough when bypasses are hidden and intermittent or located at points that are difficult to get to; hence, an alternative solution is needed to physically verify the energy discrepancy between the service connection point and the commercial meter point.

To address this problem, a low-cost dual-node wireless system was developed for local and real-time detection of electrical bypasses in low-voltage service drops. The architecture comprises two measurement nodes located at different points of the same service connection. Both nodes acquire voltage, current, active power, and accumulated energy, while Node A transmits its measurements to Node B through ESP-NOW. This configuration enables direct comparison of the electrical quantities measured upstream of the commercial meter and at the billing point without requiring a router, cellular network, or AMI infrastructure [8].

The objective of this study is to design, implement, and experimentally evaluate a two-node wireless embedded system for detecting electrical bypasses upstream of the commercial meter through synchronized differential power and energy measurements. Unlike a fixed percentage rule, the implemented decision model incorporates the estimated technical loss of the service drop and a current-dependent tolerance margin to reduce false alerts associated with conductor losses and operating variability.

The main contributions of this work are as follows: first, a dual-node embedded architecture for direct physical comparison of two points of the same low-voltage service drop; second, implementation of a loss-compensated decision model using the dynamic threshold and corrected discrepancy defined in Equations (8) and (9); third, application-layer synchronization based on sequence identification and timestamps; fourth, an experimental dataset comprising 20 controlled scenarios and 20 different residential service drops; and fifth, evaluation under high-power, transient, nonlinear-load, synchronization, and wireless-communication conditions.

2. Related Work

NTLs in electrical distribution systems have been addressed through data-based, network-based, hybrid, and inspection or instrumentation methods. Study [1] considers electricity theft as a cause of non-technical losses and analyzes its impact on the economy and operation.

On the other hand, paper [2] includes a classification method for NTLs detection methods, where data-based methods are distinguished from those based on electrical variables and network topology, as well as hybrid methods.

Smart metering systems, together with other data, are the basis of one branch of research. Along the same line, paper [3] identifies electricity theft in AMI based on the consumption patterns recorded by smart meters. Similarly, study [4] applies supervised learning to smart meter data to identify NTLs. Article [5] analyzes metering data using a time series to detect anomalies in smart metering data. These methods are applicable to situations where historical records and digital infrastructure with centralized processing capacity exist, but they are limited by the availability, quality, and representativeness of the data.

Deep learning has been applied to the classification of electricity theft patterns. Therefore, study [6] uses a wide and deep convolutional network to analyze consumption in smart grids. This method has the potential to capture multiple nonlinear relationships among large datasets. However, the method requires prior supervised training and the presence of smart meters, which are often not available in individual low-voltage connections or in environments where theft occurs before a commercial meter.

Oriented hybrid network methods combine electrical variables with topology and classification methods. Study [7] combines voltage sensitivity, power system optimization, and support vector machines to detect NTLs in smart distribution networks. Although this approach improves system observability, it requires network information, distributed measurements, and greater modeling complexity than a local solution installed in a service drop.

In low-voltage networks, some studies have incorporated distributed measurements or intermediate monitoring points. Study [9] addresses non-technical loss detection in low-voltage feeders with limited data availability. Study [10] proposes point-to-point voltage-drop measurement between smart meters to identify unauthorized consumption. Study [11] proposes a model-less method based on smart meter data, voltage sensitivity, and comparison between measured and estimated consumption. Though these methods are more aligned with the low-voltage issue, they still rely on smart meter readings, network estimates, or sensitivity parameters.

Other works investigate monitoring mechanisms closer to physical measurement between electrical points. Work [12] proposes the use of an intermediate meter for the detection of tampering, malfunctioning, and bypassing of meters in smart grids as an intrusion detection system. Work [13] presents a remote approach for the detection and identification of illegal consumers in electrical networks. Work [14] uses state estimation and variance analysis to detect irregularities in metering. These proposals provide some relevant technical criteria for the detection of NTLs; however, they usually require network infrastructure, additional metering devices, or more complex processing.

Recent studies show that low-voltage electricity theft is still an open problem. Study [15] reviews theft detection methods for low-voltage systems and notes that the location of fraud is still a problem. Paper [16] distinguishes between hardware-based and non-hardware-based approaches for detecting NTLs. Systematic review [17] further classifies detection techniques according to the algorithms they employ, their characteristics, and the associated metrics, and explains the challenges related to cost, data volume, existing infrastructure, and operation in real-world environments.

ESP-NOW enables direct communication between ESP32 devices without establishing a conventional connection through a router or access point [8]. This feature is suitable for linking two measurement points of a low-voltage service drop without AMI infrastructure, cellular communication, or a local router.

Based on the reviewed literature, the gap addressed in this work lies not only in performing local differential measurement but also in incorporating technical-loss compensation, synchronized acquisition, and acquisition-quality criteria into the decision process. Unlike approaches based primarily on historical consumption series, smart-meter networks, or network-wide state estimation, the proposed system directly evaluates two physical measurement points of an individual service connection and executes the detection logic locally.

3. Technical Basis of the Differential Balance

In a low-voltage service drop, the power supplied from the input point to a user installation does not necessarily coincide with the power recorded near the commercial meter. Under normal operation, this difference is associated with technical losses due to conductor resistance, load current, section length, and physical installation conditions.

If there exists a bypass upstream of the meter, then part of the load will be recorded at the service connection point but not necessarily at the commercial metering point; such a discrepancy shall be considered as a physical manifestation of non-technical loss.

The balance principle in use here is based on simple laws concerning electric circuits and analyses for power systems, where delivered power between any two points on a line involves resistive losses that are always present through current and equivalent resistance of a conductor [18, 19]. Under normal conditions,

Equation (1) represents the relationship between powers measured at these two different locations: one at the service connection point and another close to the commercial meter.

$$P_A \approx P_B + P_{loss} \quad (1)$$

Where P_A represents the active power measured at the service connection point, P_B represents the active power measured near the commercial meter, and P_{loss} represents the expected technical losses in the section between both points.

The primary physical indicator is the instantaneous power difference between the two nodes. This variable is defined by Equation (2).

$$\Delta P = P_A - P_B \quad (2)$$

Where ΔP corresponds to the differential power between the service drop point and the commercial meter point. Under normal operating conditions, ΔP should remain within limits that can be attributed to technical and metering losses. In cases where a load is connected upstream of the meter, P_A is greater than P_B, thus creating a difference that may be associated with a possible bypass.

To ensure that the decision criterion does not depend on an absolute power value, the difference is normalized with respect to the total active power measured at the service drop. The percentage power difference index is defined by Equation (3).

$$D_P = \frac{\max(\Delta P, 0)}{P_A} \cdot 100, P_A > 0 \quad (3)$$

where D_P is the percentage power difference with respect to the active load measured at the connection point. The term $\max(\Delta P, 0)$ prevents the classification of a bypass in the case of a negative difference due to measurement desynchronization, noise, or a temporary measurement variation.

The reference P_A is considered because it is the total power entering the evaluated installation, which includes the recorded load and any unmeasured load that may be present.

A fixed percentage criterion was initially considered as a baseline screening rule for the differential power index. Under this baseline, normal operation corresponds to $D_P \leq 5\%$, whereas values above 5% indicate a potential power discrepancy. The baseline normal-operation criterion is expressed by Equation (4).

$$D_P \leq 5\% \rightarrow \text{Normal operation} \quad (4)$$

The corresponding baseline discrepancy condition is expressed by Equation (5).

$$D_P > 5\% \rightarrow \text{Theft alert detected} \quad (5)$$

This baseline criterion is computationally simple and scales with the instantaneous active load.

However, it does not explicitly compensate for the effect of conductor resistance and load current, which can produce significant technical losses under high-demand conditions. Therefore, the final experimental classification used in this study was based on the loss-compensated dynamic model defined by Equations (8) and (9), rather than on the fixed 5% criterion alone.

The accumulated energy discrepancy allows the temporal evolution of the difference between the two measurement points to be analyzed.

This complementary variable is defined by Equation (6).

$$\Delta E = E_A - E_B \tag{6}$$

Where E_A represents the accumulated energy measured at the service connection point and E_B represents the accumulated energy measured near the commercial meter. While ΔP and D_P allow an instantaneous alert to be activated, ΔE allows unrecorded energy to be documented during an evaluation window.

The resistive losses of the service drop section can be approximated by the Joule-effect relationship between current and the equivalent resistance of the conductor [18, 19]. This relationship is expressed by Equation (7).

$$P_{loss} = I^2 R_{line} \tag{7}$$

Where I represents the current flowing through the conductor and R_{line} represents the equivalent resistance of the evaluated section. This relationship explains why technical losses increase quadratically with current and can be significant in longer service drops or under high load.

To reduce false positives under high-current conditions, the detection model incorporates the expected technical loss of the service drop into a dynamic threshold dependent on the measured current and the equivalent conductor resistance.

This improvement is expressed by Equation (8).

$$\Delta P_{thresh,dyn}(I) = I_B^2 R_{line} + \sigma \tag{8}$$

Where I_b represents the current measured at Node B, R_{line} represents the equivalent resistance of the evaluated service-drop conductor, and σ represents an adaptive tolerance margin associated with measurement and short-term operating variability. The $I_B^2 R_{line}$ The term accounts for the expected resistive loss of the conductor, preventing this physical loss from being interpreted directly as a non-technical loss.

A percentage discrepancy corrected by estimated technical losses can also be defined. This index is presented in Equation (9).

$$D_{P,corr} = \frac{\max(\Delta P - I_B^2 R_{line}, 0)}{P_A} \cdot 100 \tag{9}$$

where $D_{P,corr}$ represents the percentage power discrepancy after subtracting the estimated technical line loss. In the implemented model, the measured ΔP is compared with $\Delta P_{thresh,dyn}$. A bypass alert is generated only when the measured power difference exceeds the dynamic threshold for three consecutive valid samples. $D_{P,corr}$ is retained as a complementary normalized indicator of the residual discrepancy after technical-loss compensation. Figure 1 represents the differential balance principle used by the system, where Node A measures the total power and energy at the service drop, whereas Node B records the electrical variables near the commercial meter.

Table 1 summarizes the electrical indicators used in the detection model, including instantaneous power variables, percentage indices, and the accumulated energy discrepancy.

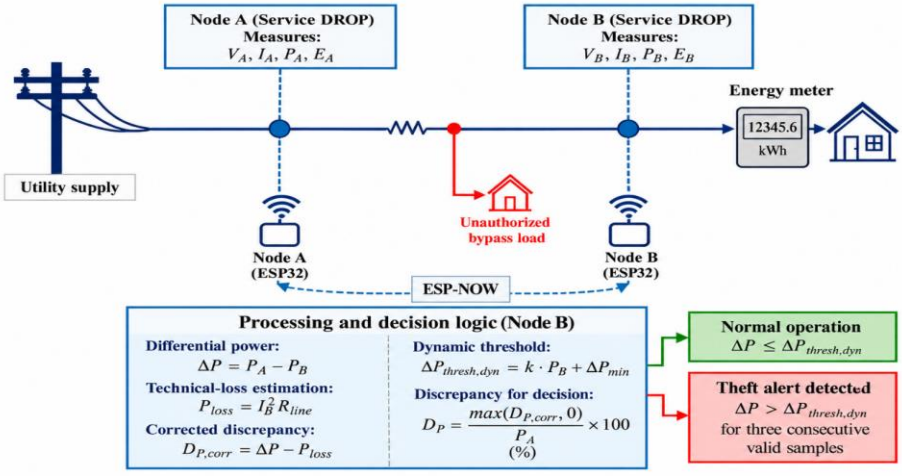


Fig. 1 Differential power and energy balance diagram for bypass detection in low-voltage service drops

Table 1. Main indicators used in the differential detection model

Indicator	Unit	Function in the detection model	Operational interpretation
(P_A)	W	Measures active power at the service drop	Total active power entering the evaluated supply
(P_B)	W	Measures active power near the commercial meter	Active power registered at the metering point
(ΔP)	W	Real-time differential indicator	Instantaneous power discrepancy between the two nodes
D_P	%	Relative detection indicator	Percentage discrepancy with respect to active input power
E_A	Wh	Measures accumulated energy at the service drop	Total accumulated energy entering the evaluated supply
E_B	Wh	Measures accumulated energy near the meter	Accumulated energy registered at the metering point
ΔE	Wh	Cumulative discrepancy indicator	Energy difference during the test window
$(\Delta P_{thresh,dyn})$	W	Implemented a dynamic threshold	Current-dependent threshold incorporating estimated technical loss and adaptive tolerance
$(D_{P,corr})$	%	Implemented corrected discrepancy index	Relative discrepancy after compensation for estimated technical losses

4. Proposed System

4.1. General System Architecture

The proposed system is a low-cost dual-node wireless architecture to detect electrical bypasses in low-voltage service drops. The solution comprises two measurement nodes: one at the service drop point and another next to the commercial meter. With this setup, it becomes possible to compare electrical variables measured before and after a potential bypass point.

The architecture includes a measurement point upstream of the commercial meter; if any load connects before the metering system meant for billing, that load will be recorded by the service drop node, but not by the node next to the meter. This difference enables the application of the differential balance criterion described in Section 3.

The design was defined under three technical requirements: low cost, independence from external communication infrastructure, and local real-time operation. To satisfy these needs, ESP32 microcontrollers were used along with PZEM-004T V3 modules implemented on top of ESP-NOW communication using MicroPython firmware. Figure 2 shows the functional architecture connecting Node A, Node B, the ESP-NOW wireless link, and the local visualization interface.

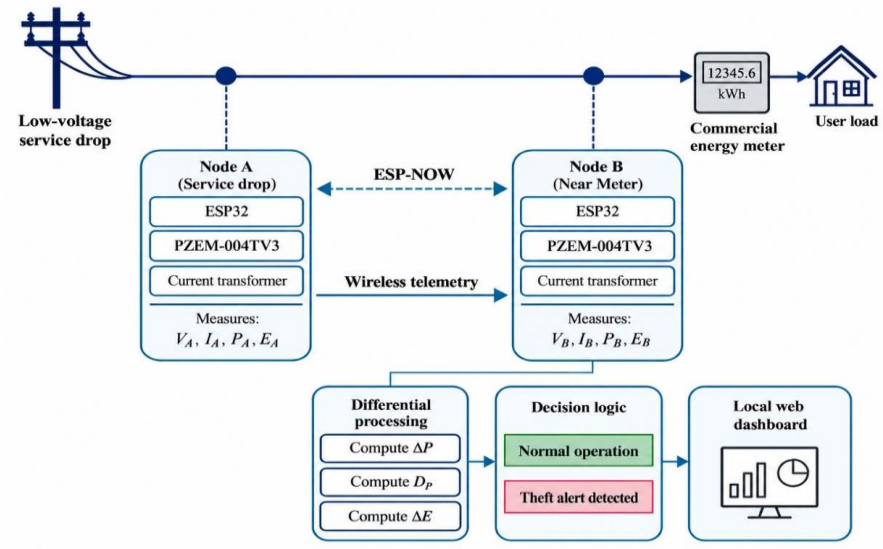


Fig. 2 Functional architecture diagram of the proposed dual-node wireless system

4.2. Service Drop Node and Meter Node

The Connection Node, or Node A, is installed at the electrical supply point or in the section before the commercial meter. It measures the total energy and power supplied to the respective installations. Since it is installed before the commercial meter and before an unauthorized branch, this node forms a measurement boundary.

Node A is composed of an ESP32, a PZEM-004T V3 module, a non-invasive current transformer, a level-shifting circuit, and a power supply circuit. The PZEM-004T V3 measures voltage, current, active power, and energy. ESP32 processes the measured parameters and transmits the values V_A, I_A, P_A, and E_A to Node B through ESP-NOW. The Meter Node, or Node B, is installed next to the commercial meter.

It acquires the local electrical variables, receives the telemetry transmitted by Node A, and executes the embedded detection algorithm.

Node B calculates ΔP, estimates the technical line loss, and evaluates $D_{P,corr}$ and $\Delta P_{thresh,dyn}$, records ΔE, classifies the operating condition, and updates the local web interface. The function of each measurement node, its location, and the electrical parameters measured or processed by the system are summarized in Table 2.

Table 2. Functional description of the proposed measurement nodes

Node	Location	Main function	Measured or processed variables
Node A	Service drop point	Measures total electrical input to the evaluated installation	(V_A), (I_A), (P_A), (E_A)
Node B	Near the commercial energy meter	Measures local variables, receives Node A data and executes the detection algorithm	(V_B), (I_B), (P_B), (E_B), (ΔP), (D_P), (ΔE), $(D_{P,corr})$, $(\Delta P_{thresh,dyn})$, (P_{loss})

4.3. Electrical Instrumentation and Wireless Communication

The measurement of electrical variables in both nodes was performed using PZEM-004T V3 modules. Communication between the PZEM-004T V3 and the ESP32 was implemented through UART under the Modbus RTU protocol at 9600 bps. Because the ESP32 operates with 3.3 V logic levels and the PZEM-004T V3 requires 5 V TTL levels for serial communication, a bidirectional logic-level converter was incorporated. Figure 3 presents the electrical connection among the ESP32, the bidirectional logic-level converter, and the PZEM-004 TV3 module, used to condition UART communication between 3.3 V and 5 V devices.

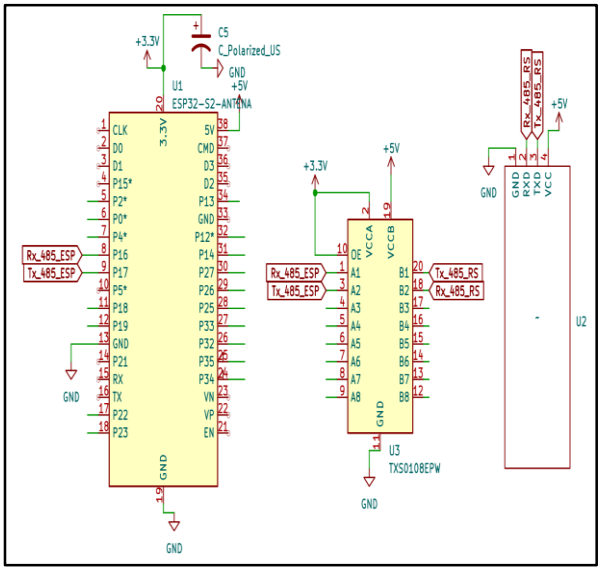
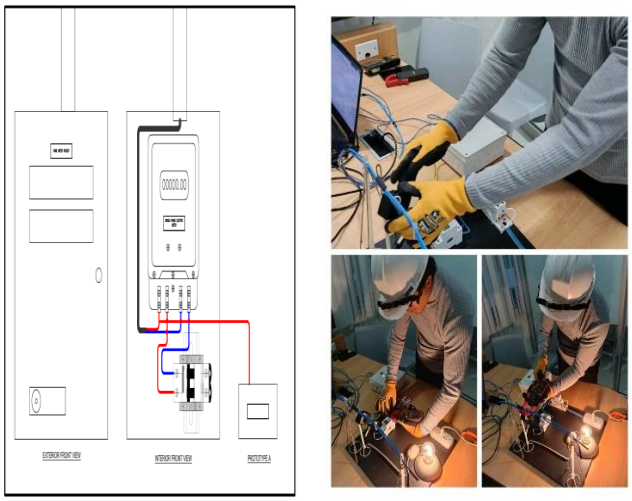


Fig. 3 Electrical wiring diagram between ESP32, logic level converter and PZEM-004T V3

From a physical perspective, the prototype was designed to operate next to the commercial meter and the associated protection board. Figure 4(a) shows the location of the device in the board, considering the commercial single-phase meter, the C60 circuit breaker, and the exterior and interior views of the panel. Figure 4(b) presents the preliminary verification of the prototype through a pilot test using a lamp as a representative load prior to its field installation.



(a) **(b)**

Fig. 4 Physical installation and pilot testing of the proposed prototype. (a) Prototype location near the commercial single-phase energy meter and the associated protection board, and (b) Preliminary pilot test using a light bulb as a representative load before field installation.

Communication between Node A and Node B was implemented through ESP-NOW in the 2.4 GHz band without requiring a conventional TCP/IP connection or an external

access point [8]. During each experimental scenario, wireless-link quality was characterized by recording the Received Signal Strength Indicator (RSSI), the number of transmitted and received packets, Packet Error Rate (PER), and transmission latency. Measurements were obtained over windows of 1000 transmitted packets. A wireless acquisition was considered acceptable when PER ≤ 5% and transmission latency ≤ 20 ms, whereas RSSI was retained as a descriptive indicator of link quality.

4.4. Firmware, Visualization, and Synchronization

The firmware runs in MicroPython. Node A acquires the electrical variables from the PZEM-004T V3, packages the measurements, and periodically transmits them to Node B through ESP-NOW. Each transmitted acquisition is associated with a sequence identifier and timestamp. Node B associates the received measurement with its local acquisition and records the temporal offset Δt between both measurements.

Node B estimates the technical line loss, calculates ΔP, and $D_{P,corr}$, evaluates $\Delta P_{thresh,dyn}$, and records the accumulated-energy difference ΔE. A bypass alert is generated when ΔP exceeds the dynamic threshold for three consecutive valid samples. Non-blocking processing was used to reduce interference between electrical acquisition, wireless reception, and web-interface requests.

Synchronization was implemented at the application layer through sequence identification and timestamp-based pairing. A measurement pair was considered valid when Δt ≤ 50 ms under stable-load conditions and Δt ≤ 30 ms under dynamic-load conditions. Acquisitions exceeding these limits were marked for repetition and excluded from classification-performance calculations.

The local web interface displays the electrical variables measured by both nodes together with the differential indicators and operating status. The alert state is updated only after the dynamic decision criterion has been satisfied for three consecutive valid samples. Figure 5 presents the real-time monitoring interface implemented in Node B, where the local web server displays the electrical variables of both nodes, the power difference, the percentage discrepancy, the accumulated energy, and the operating status. When ΔP exceeds $\Delta P_{thresh,dyn}$ For three consecutive valid samples, the dashboard changes to the theft-alert condition.

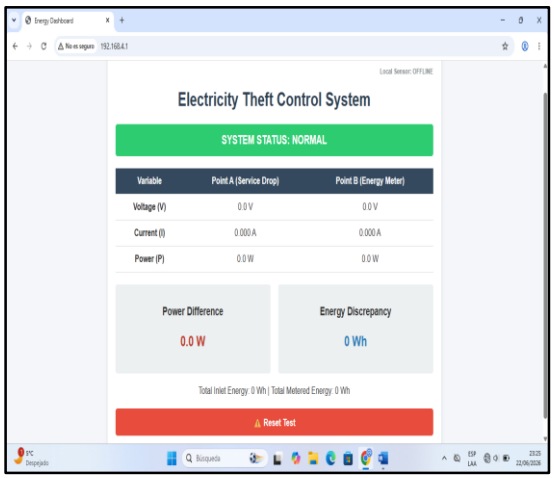


Fig. 5 Local web dashboard for real-time monitoring and theft alert visualization

Table 3 summarizes the functional subsystems of the prototype, distinguishing service drop measurement, meter-side measurement, wireless communication, embedded processing, visualization, and test synchronization.

Table 3. Functional summary of the proposed system subsystems

Subsystem	Main elements	Function
Boundary measurement subsystem	Node A, ESP32, PZEM-004T V3, current transformer	Measures electrical variables at the service drop
Meter-side measurement subsystem	Node B, ESP32, PZEM-004T V3, current transformer	Measures electrical variables near the commercial meter
Wireless communication subsystem	ESP32, ESP-NOW	Transfers telemetry from Node A to Node B
Embedded processing subsystem	ESP32, MicroPython firmware	Calculates differential indicators and classifies system status
Visualization subsystem	Local web dashboard, JSON/AJAX	Displays measurements and alert conditions
Synchronization subsystem	Sequence identifiers and timestamps	Pair Node A and Node B measurements from the same acquisition interval and record the temporal offset Δt

5. Materials and Methods

5.1. Experimental Design

The experimental campaign was structured to evaluate the detection system under controlled and residential field conditions. A total of 40 scenarios were considered, divided into 20 controlled tests and 20 different residential service drops. The controlled group comprised 10 normal operating conditions and 10 controlled bypass conditions, whereas the field group comprised 20 residential connections evaluated without deliberate bypass intervention.

The evaluated conditions included conductor cross-sectional areas of 6 and 10 mm², service-drop lengths from 4 to 25 m, bypass powers from 30 to 1000 W, and different resistive, electronic, motor-driven, nonlinear, mixed, and high-power loads. The field scenarios included urban, peri-urban, and rural environments. Before a scenario was included in the classification-performance calculation, synchronization and communication-quality criteria were verified. Acquisitions that did not satisfy these requirements were marked for repetition instead of being counted as valid classification outcomes. Figure 6 summarizes the methodological sequence followed during system implementation and experimental validation.

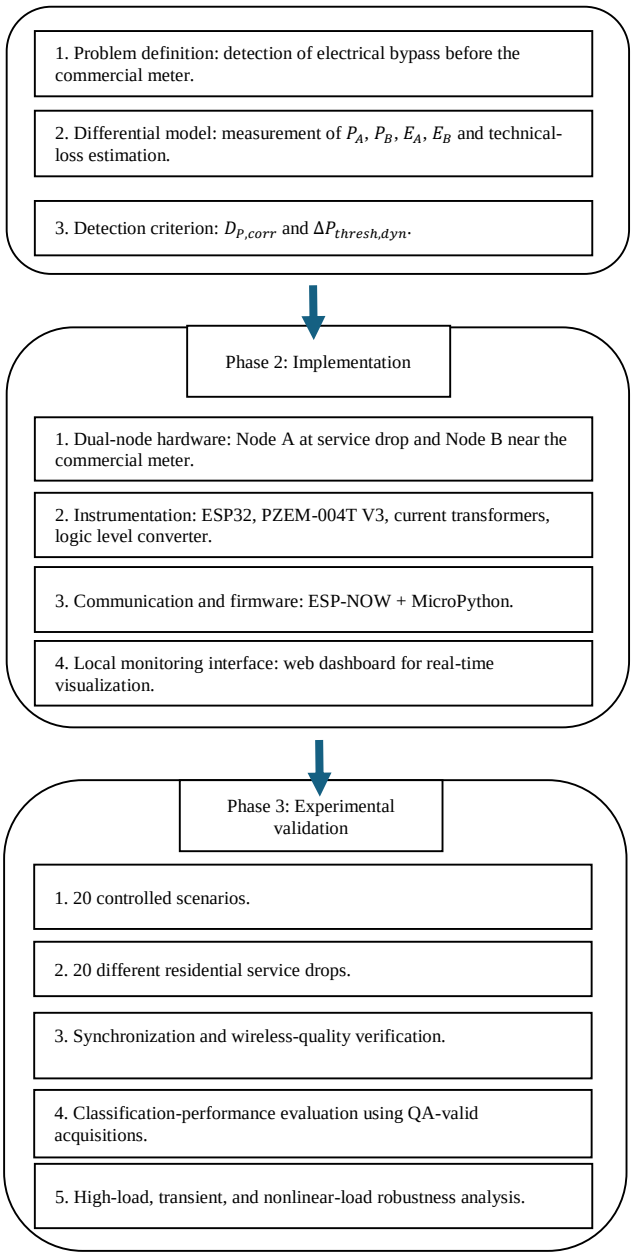


Fig. 6 Methodological flow diagram for design, implementation and experimental validation

5.2. Evaluated Scenarios and Residential Service Drops

The experimental dataset comprised 40 scenarios: 20 controlled tests and 20 different residential service drops. The controlled group included 10 normal operating conditions and 10 controlled bypass events. The bypass power ranged from 30 to 1000 W, and the event duration ranged from 20 to 120 s. The 20 field scenarios were performed on residential service drops without deliberate bypass intervention and were used primarily to evaluate normal-operation robustness and false-positive behavior.

The evaluated service drops used conductor cross-sectional areas of 6 and 10 mm² and lengths from 4 to 25 m. Load profiles included resistive loads, switched-mode power supplies, motors, refrigeration equipment, washing-machine operation, mixed residential loads, nonlinear electronic loads, and high-power conditions above 5 kW. The field scenarios covered urban, peri-urban, and rural environments.

A complementary accumulated-energy test was also conducted over seven days. Because only one prolonged observation was available and no bypass event occurred during that interval, this test was retained as a functional verification of continuous operation rather than as statistical evidence of long-term detection reliability.

Table 4. Experimental classification dataset

Experimental group	N	Operating conditions	Purpose
Controlled tests	20	10 normal + 10 controlled bypass	Detection, technical-loss compensation, transient, nonlinear-load, and bypass evaluation
Residential field tests	20	20 different service drops without deliberate bypass	Field robustness and false-positive evaluation
Total	40	-	Expanded experimental dataset

The tests were carried out in two modalities. The first one was instantaneous power tests, where the system counted ΔP and D_P during the acquisition and classification cycle. The second one was a complementary accumulated-energy difference test, with the equipment installed for seven days; this long test served as a functional check of continuous operation. The result was negative for an attempt at electricity theft during the evaluated window.

The loads used corresponded to real domestic equipment. Televisions of 40 inches with an approximate maximum consumption of 840 W, electric showers of 5200 W,

incandescent lamps of 25 W, 50 W, and 100 W, sound systems of 350 W, laptops of 230 W, a washing machine of 1100 W, and other residential equipment were considered. Table 5 details the domestic loads used during the tests.

Table 5. Domestic loads considered during the experimental tests

Load type	Approximate active power	Load condition
Incandescent lamp	25 W, 50 W, 100 W	Low-power residential load
Laptop	230 W	Low-to-medium residential load
Sound system	350 W	Medium residential load
Television	Up to 840 W	Medium residential load
Washing machine	1100 W	Medium-to-high residential load
Electric shower	5200 W	High-power residential load
Additional domestic equipment	Variable	Real household operating condition

5.3. Classification Criterion and Experimental Configuration

The final bypass classification was based on the dynamic threshold defined in Equation (8), rather than on the fixed 5% criterion alone. For each acquisition, the system obtained electrical variables from Nodes A and B, estimated the expected technical line loss, and calculated $D_{P,corr}$ According to Equation (9), and compared the measured ΔP with $\Delta P_{thresh,dyn}$.

A bypass alert was generated only when ΔP exceeded the corresponding dynamic threshold for three consecutive valid samples. The accumulated-energy difference ΔE was retained as a complementary indicator for prolonged monitoring and was not used as the primary instantaneous classification variable. The classification criteria applied during the experimental evaluation are summarized in Table 6.

Table 6. Detection criteria used in the experimental validation

Condition	Classification criterion	System status
Normal operation	$\Delta P \leq \Delta P_{thresh,dyn}$	Normal operation
Possible bypass condition	$\Delta P > \Delta P_{thresh,dyn}$ for three consecutive valid samples	Theft alert detected
Complementary energy verification	Evaluation of accumulated (ΔE) during prolonged operation	Functional verification

Each node used an ESP32 and a PZEM-004 V3 module to acquire voltage, current, active power, and accumulated energy. Communication between the ESP32 and the PZEM-004T V3 was performed by UART with Modbus RTU at 9600 bps. A bidirectional 3.3 V to 5 V converter was used to condition the serial communication signals. Table 7 summarizes the main components of the prototype, specifying the quantity used and the function of each element within the measurement and communication system.

Table 7. Main components used in the experimental implementation

Component	Quantity	Function
ESP32 development board	2	Embedded processing and wireless communication
PZEM-004T V3	2	Voltage, current, active power and energy measurement
Current transformer	2	Non-invasive current measurement
Logic level converter	2	UART signal conditioning between ESP32 and PZEM-004T V3
Power supply stage	2	Electrical supply for each node
Local web interface	1	Real-time monitoring and alert visualization

Node A transmitted V_A, I_A, P_A, and E_A to Node B through ESP-NOW. Node B received this information and acquired its local variables. (V_B, I_B, P_B, E_B), calculated ΔP, D_P Moreover, ΔE, and classified the operating status. Table 8 presents the experimental configuration parameters used in the tests, including wireless protocol, sensor communication, detection criterion, firmware language, and total number of trials.

Table 8. Experimental configuration parameters

Parameter	Value
Wireless protocol	ESP-NOW
Wireless band	2.4 GHz
Sensor communication protocol	UART / Modbus RTU
UART baud rate	9600 bps
Detection criterion	Dynamic threshold with three consecutive valid exceedances
Firmware language	MicroPython
Web update method	JSON/AJAX
Controlled scenarios	20
Residential field scenarios	20
Total evaluated scenarios	40
QA-valid acquisitions	38
Conductor cross-	6 and 10 mm²

sectional areas	
Service-drop lengths	4–25 m
Controlled bypass range	30–1000 W
Controlled bypass duration	20–120 s

5.4. Experimental Procedure

The experimental procedure included sensor verification, wireless-link assessment, prototype installation, synchronized electrical acquisition, application of acquisition-quality criteria, classification recording, and complementary accumulated-energy monitoring. Table 9 summarizes the principal stages.

Table 9. Experimental procedure

Stage	Description
Sensor verification	Verification of PZEM-004T V3 readings in both nodes
Wireless communication test	Recording of RSSI, transmitted and received packets, PER, and transmission latency over 1000-packet windows.
Prototype installation	Installation of Node A at the service-drop side and Node B near the commercial meter
Synchronized acquisition	Pairing of measurements using sequence identifiers and timestamps, and recording of Δt
Technical-loss evaluation	Estimation of line loss and calculation of the loss-corrected indicators
Accumulated energy test	Complementary 7-day verification using (ΔE)

False. During each acquisition cycle, the telemetry received from Node A was associated with the local measurement of Node B. Measurement pairs were accepted when $\Delta t \leq 50$ ms under stable-load conditions and $\Delta t \leq 30$ ms under dynamic-load conditions.

Wireless acquisitions were accepted when PER ≤ 5% and latency ≤ 20 ms. Records outside the established quality limits were marked for repetition and excluded from the classification-performance calculation.

5.5. Metrological Characterization and Uncertainty Analysis

The two PZEM-004T V3 measurement channels were evaluated as part of the differential acquisition system under different operating conditions. The analysis considered resistive, reduced-power-factor, dynamic, and nonlinear loads because these conditions can increase variability between measurements obtained at separated electrical points. Measurement uncertainty and short-term operating variability were incorporated into the adaptive tolerance term used by the dynamic threshold. This prevents normal differences attributable to measurement dispersion, conductor losses, or short-term load variations from being interpreted directly as evidence of a non-technical loss.

A complete traceable calibration against a certified power-quality analyzer, including formal calibration curves and a metrological uncertainty budget, was not established in the present experimental campaign. Therefore, the prototype is evaluated as a bypass-detection and local energy-auditing system rather than as a certified metrological instrument.

5.6. Evaluation Metrics

No metrological characterization was performed with a certified reference instrument. Therefore, absolute errors in voltage, current, or power compared with reference equipment cannot be reported.

The analysis is limited to the functionality of the prototype, the consistency of the differential balance, and event classification. Evaluation metrics used to assess system performance in the context of the experimental confusion matrix are summarized in Table 10.

Table 10. Evaluation metrics used in the experimental validation

Metric	Expression	Description
Accuracy	((TP+TN)/ (T+TN+FP+FN))	Proportion of correct classifications
Sensitivity / Recall	(TP/(TP+FN))	Ability to detect theft or bypass conditions
Specificity	(TN/(TN+FP))	Ability to identify normal operation
Precision	(TP/(TP+FP))	Reliability of generated theft alerts

Note: TP: True Positive; TN: True Negative; FP: False Positive; FN: False Negative.

6. Results

6.1. Representative Dashboard Results

Figures 7-10 present representative outputs of the local web dashboard obtained during functional verification of the prototype. These examples illustrate the visualization of the electrical variables measured by both nodes, the instantaneous power difference, the percentage discrepancy, the accumulated-energy difference, and the operating status.

The dashboard examples are presented for interface verification and are not used independently to calculate the classification metrics reported in Section 6.2. Figure 7 shows a representative normal-operation condition without an electrical bypass. Node A recorded 34.3 W and Node B recorded 33.6 W, resulting in a power difference of 0.7 W, equivalent to 2.04%. The dashboard displayed the corresponding normal operating status.

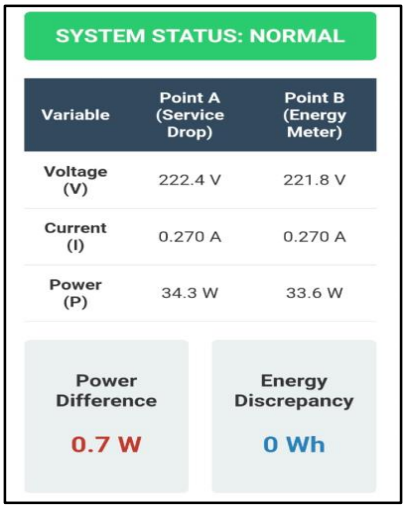


Fig. 7 Local web dashboard under normal operation without electrical bypass

Figure 8 shows the local dashboard during an electrical bypass condition, in an example case using a blender. In this instance, Node A recorded a substantially higher value than the commercial meter reading. Specifically, Node A was 1599.2 W, and Node B was 141.2 W; hence, the difference was 1458.0 W or 91.17%. The total energy difference equated to 18 Wh.

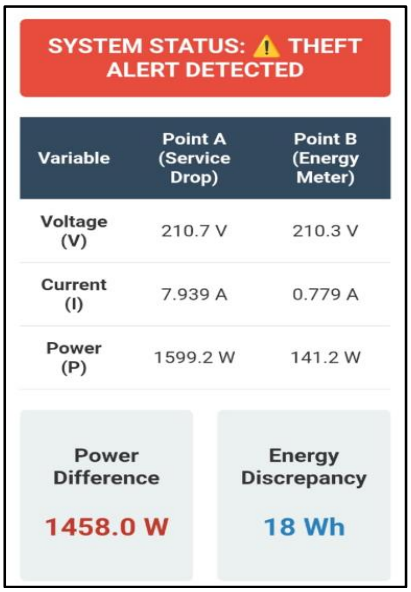


Fig. 8 Local web dashboard under electrical bypass condition using a blender load

Figure 9 shows the local dashboard under a bypass condition with a medium-power load, where the percentage discrepancy exceeded the 5% threshold even though the absolute power difference was lower than in high-demand scenarios. In this case, Node A recorded 1142.9 W, and Node B recorded 906.7 W. The difference was 236.2 W, equivalent to 20.67%, with an energy discrepancy of 8 Wh.

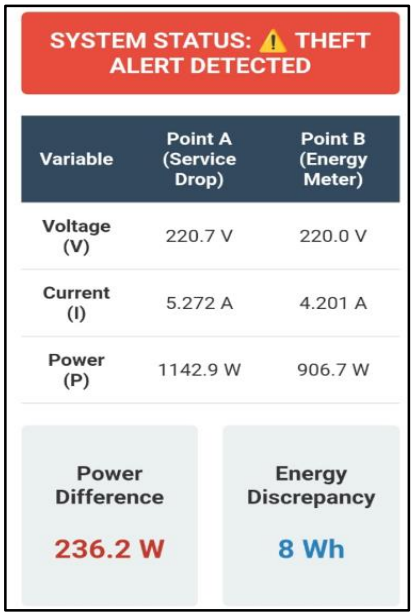


Fig. 9 Local web dashboard under electrical bypass condition using a medium-power load

Figure 10 shows the local dashboard under a bypass condition with a microwave load, where the difference between P_A and P_B activated the possible electricity theft alert. Node A recorded 1413.6 W, and Node B recorded 141.1 W. The difference was 1272.5 W, equivalent to 90.02%, with an energy discrepancy of 10 Wh.

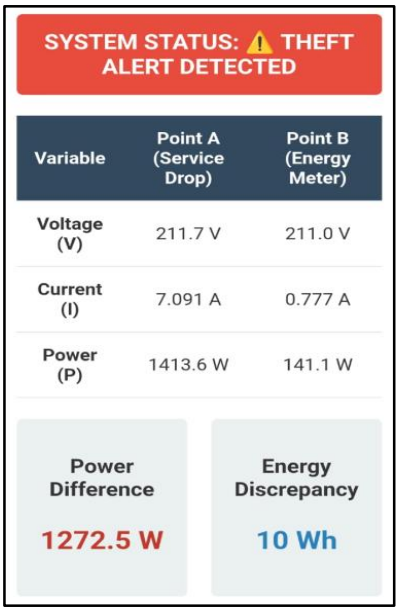


Fig. 10 Local web dashboard under electrical bypass condition using a microwave load

Table 11 consolidates the representative results from the local dashboard, including electrical variables, differential power, percentage discrepancy, and accumulated energy for normal and bypass conditions.

Table 11. Representative differential power results under normal and bypass conditions

Test scenario	System status	(V_A) (V)	(V_B) (V)	(I_A) (A)	(I_B) (A)	(P_A) (W)	(P_B) (W)	(ΔP) (W)	(D_P) (%)	(ΔE) (Wh)
Normal operation without bypass	Normal	222.4	221.8	0.270	0.270	34.3	33.6	0.7	2.04	0
Bypass with blender load	Theft alert detected	210.7	210.3	7.939	0.779	1599.2	141.2	1458.0	91.17	18
Bypass with a medium-power load.	Theft alert detected	220.7	220.0	5.272	4.201	1142.9	906.7	236.2	20.67	8
Bypass with microwave load.	Theft alert detected	211.7	211.0	7.091	0.777	1413.6	141.1	1272.5	90.02	10

6.2. Confusion Matrix and Performance Metrics

Forty scenarios were executed during the experimental campaign. Two acquisitions did not satisfy the established acquisition-quality criteria and were marked for repetition.

Scenario C09 exceeded the temporal-offset limit established for dynamic loads, whereas scenario V20 exceeded the wireless PER and latency limits. Consequently, the classification metrics were calculated from the 38 QA-valid acquisitions.

Among these acquisitions, the system yielded 9 True Positives (TP), 28 True Negatives (TN), 0 False Positives (FP), and 1 False Negative (FN). The false-negative case corresponded to scenario C11, which involved the lowest controlled bypass power of 30 W.

Based on these results, the system achieved an accuracy of 97.37%, a sensitivity of 90.00%, a specificity of 100.00%, and a precision of 100.00%. Table 12 presents the confusion matrix obtained from experimental tests.

Table 12. Confusion matrix obtained from the experimental tests

Actual condition / System classification	Theft alert detected	Normal operation	Total
Bypass condition	9	1	10
Normal condition	0	28	28
Total	9	29	38

Table 13 presents the performance metrics calculated from the confusion matrix, including accuracy, sensitivity, specificity, and precision.

Table 13. Classification performance metrics

Metric	Result
Accuracy	97.37%
Sensitivity / Recall	90.00%
Specificity	100.00%
Precision	100.00%

6.3. Experimental Validation of the Loss-Corrected Decision Model

Equations (8) and (9) were applied during the experimental campaign to evaluate whether the measured difference between Nodes A and B could be explained by the expected technical loss of the service drop. For each QA-valid acquisition, the technical line loss was estimated from the measured current and conductor resistance, the residual discrepancy after loss compensation was obtained, and the measured ΔP was compared with $\Delta P_{thresh,dyn}$. Table 14 presents representative cases. In scenario C05, corresponding to normal operation above 5 kW, the measured power difference was 83.04 W, and the estimated technical loss was 81.09 W, leaving a residual of 1.94 W after loss compensation. Scenario C10 produced a measured difference of 68.06 W and an estimated technical loss of 62.11 W, leaving a residual of 5.95 W. Under controlled bypass conditions, scenario C12 produced a measured difference of 151.30 W and a residual of 150.19 W after loss compensation, whereas scenario C14 produced a measured difference of 419.95 W and a residual of 403.80 W. Both exceeded their corresponding dynamic thresholds and were classified as bypass events. Five QA-valid normal-operation scenarios above 5 kW, identified as C05, C10, V17, V18, and V19, were classified as normal. No false-positive event was recorded within this high-load subset.

Table 14. Representative validation of the loss-corrected decision model

Scenario	Operating condition	ΔP (W)	P_{loss} (W)	Residual after loss compensation (W)	$\Delta P_{thresh,dyn}$ (W)	Classification
C05	High load without bypass	83.04	81.09	1.94	157.54	Normal
C10	High load without bypass	68.06	62.11	5.95	148.96	Normal
C12	Controlled bypass	151.30	1.11	150.19	21.11	Alert
C14	Controlled bypass	419.95	16.15	403.80	50.74	Alert

6.4. Synchronization and Acquisition Quality

The temporal offset between paired measurements from Nodes A and B was evaluated as an acquisition-quality parameter. Thirty-nine of the 40 scenarios satisfied the established synchronization criterion. Among the accepted measurement pairs, Δt ranged from 3.27 to 18.89 ms, with a mean value of 11.19 ms.

Scenario C09 involved a dynamic motor load and produced a temporal offset of 62 ms, exceeding the 30 ms limit established for dynamic conditions. This acquisition was therefore marked for repetition and excluded from the valid classification set. The timestamp- and sequence-based pairing procedure allowed this asynchronous acquisition to be identified before the resulting alert was considered a valid false-positive event.

6.5. Wireless Link Performance

The ESP-NOW link was evaluated using RSSI, PER, and transmission latency over the 40 experimental scenarios. A total of 40,000 packets were transmitted, and 39,685 were received, corresponding to an overall PER of 0.79%. RSSI ranged from −83.61 to −44.86 dBm, with a mean value of −64.42 dBm.

The mean transmission latency was 4.36 ms. Thirty-nine scenarios satisfied the wireless criteria of PER ≤ 5% and latency ≤ 20 ms. Scenario V20 presented a PER of 5.8% and a latency of 22 ms and was therefore marked for repetition. The wireless-link performance metrics obtained during the experimental evaluation are summarized in Table 15.

Table 15. ESP-NOW wireless-link performance

Metric	Result
Transmitted packets	40,000
Received packets	39,685
Overall PER	0.79%
RSSI range	−83.61 to −44.86 dBm
Mean RSSI	−64.42 dBm
Mean latency	4.36 ms
Maximum latency	22.00 ms
Scenarios satisfying wireless criteria	39/40

6.6. Transient and Non-Linear Load Immunity

Dynamic and nonlinear operating conditions were included to evaluate whether rapid load variations could produce spurious bypass detections. Thirteen no-bypass scenarios involved dynamic loads, including motor starting, switched-mode power supplies, refrigeration, washing-machine operation, rapid load steps, and mixed motor-electronic loads. Twelve of these scenarios satisfied the acquisition-quality criteria and were correctly classified as normal operation. Scenario C09 was excluded because its temporal offset exceeded the established synchronization limit and was therefore marked for repetition rather than considered a valid false-positive event.

Eight no-bypass scenarios included nonlinear electronic loads, and all QA-valid acquisitions were classified as normal. In addition, controlled bypass scenarios C13 and C17 included nonlinear loads, while C19 incorporated a motor-driven load; all three were correctly classified as bypass events. These results indicate that the decision criterion remained stable under the evaluated transient and nonlinear-load conditions when synchronization and communication-quality requirements were satisfied.

6.7. Field Installation Verification

Figure 11 shows the preliminary installation of the service drop node in a low-voltage environment, used to verify the physical feasibility of locating the system in the field.



Fig. 11 Preliminary field installation of the service drop node in a low-voltage environment

Figure 12 shows the location of the prototype next to the commercial metering system, evidencing the installation of the node associated with the billing point.



Fig. 12 Prototype installation near the commercial energy meter

7. Discussion

7.1. Interpretation of the Experimental Results

The experimental results indicate that the dual-node architecture can identify power discrepancies associated with electrical bypasses while accounting for technical line losses and acquisition quality. Among the 38 QA-valid acquisitions, the system obtained 9 true positives, 28 true negatives, no false positives, and one false negative. This resulted in an accuracy of 97.37%, sensitivity of 90.00%, specificity of 100.00%, and precision of 100.00%. The absence of false positives among the valid normal-operation acquisitions indicates that the loss-compensated decision criterion reduced the influence of technical conductor losses within the evaluated conditions. This behavior was particularly relevant in the QA-valid normal scenarios above 5 kW, all of which remained correctly classified.

The single false negative occurred with the 30 W bypass condition in scenario C11. In this case, the residual discrepancy after compensation remained below the adaptive tolerance margin. This result identifies a practical lower detection limit and shows the trade-off between reducing false-positive sensitivity and detecting very low-power bypass events. The two records excluded by the QA criteria were treated as acquisition-quality failures rather than classification errors. This distinction prevents desynchronization or inadequate wireless communication from being interpreted as detection performance.

7.2. Comparison with Data-based, AMI, and Machine Learning Methods

The proposed system differs from methods based on AMI and historical consumption analysis. Studies [3-5] identify suspicious consumption patterns from smart-meter records, whereas the present approach performs direct physical comparison between two measurement points of the same service drop. This configuration allows discrepancies upstream of the commercial meter to be evaluated without requiring historical customer-consumption data.

Machine-learning and deep-learning approaches such as [4, 6, 7] can identify complex patterns over large datasets but require representative training data, event labels, smart-meter infrastructure, or network information. In contrast, the proposed system executes a low-complexity physical decision model locally on ESP32 microcontrollers. Its function is therefore complementary to large-scale classifiers: it provides local verification of a specific service connection rather than population-level screening.

7.3. Comparison with Hybrid Methods and Distributed Measurement

Network-oriented hybrid approaches combine electrical measurements with network models, optimization, parameter estimation, or machine-learning techniques. Studies [7] and [9-11] provide broader network-level information but require smart meters, network parameters, or additional processing infrastructure. Studies [12-14] provide a closer comparison because they incorporate intermediate electrical measurements, remote monitoring, or network-state information for NTL detection. The proposed system operates at the individual service-drop level using two embedded measurement nodes and direct ESP-NOW communication. It does not require state estimation of the complete distribution network, historical customer databases, cellular communication, or a local router.

The proposed system achieved an accuracy of 97.37% over the QA-valid acquisition set, while the wireless link showed an overall PER of 0.79% and a mean transmission latency of 4.36 ms. Direct numerical ranking against the cited methods is not performed because their datasets, fraud conditions, system boundaries, and validation protocols differ. The principal distinction of the proposed architecture is the combination of direct dual-point measurement, local processing, technical-loss compensation, and acquisition-quality control at an individual low-voltage service connection.

According to reviews [15-17], the main constraints for detecting NTLs are the cost of the required infrastructure, data availability, the difficulty of locating fraud, and false positives. The result of this research is in line with the previously mentioned constraints: the system detected all conditions that were intentionally established to create a fraud scenario, but two false positives were generated in the case of a long service connection with a high load.

7.4. Analysis of Technical-Loss Compensation

Technical line losses directly influence the power difference measured between Nodes A and B, particularly as conductor current and resistance increase. For this reason, the implemented decision model incorporates the expected I^2R loss into the dynamic threshold rather than interpreting the complete measured difference as evidence of a non-technical loss.

The effect of this compensation can be observed in scenarios C05 and C10. Although their measured power differences were 83.04 W and 68.06 W, respectively, most of these differences were explained by estimated conductor losses. After compensation, the remaining residuals were 1.94 W and 5.95 W, and both scenarios were correctly classified as normal.

The same behavior was observed in the five QA-valid normal-operation scenarios above 5 kW, none of which produced a false-positive alert. These results show that technical-loss compensation reduced false-positive susceptibility within the evaluated range of conductor sections, service-drop lengths, and load levels.

7.5. Limitations and Future Work

The seven-day accumulated-energy test was retained as a complementary verification of continuous operation. Because only one prolonged observation period was available and no bypass event occurred during this interval, long-term sensitivity and false-alarm probability cannot be inferred from this test. Repeated long-duration evaluations, including normal operation, controlled bypass events, intermittent bypasses, and varying load profiles, are required.

The experimental campaign included 20 different residential service drops with conductor cross-sectional areas of 6 and 10 mm² and lengths from 4 to 25 m. Therefore, the reported findings should not be extrapolated to substantially longer service drops, other conductor configurations, or multiphase installations without additional validation.

Although RSSI, PER, transmission latency, and temporal offset were evaluated, line-of-sight and wall-obstructed propagation conditions were not investigated separately. Payload encryption and resilience against intentional jamming or spoofing were also not experimentally assessed. These aspects require a dedicated wireless-reliability and cybersecurity study.

A complete traceable metrological characterization of both PZEM-004T V3 measurement channels against a certified power-quality analyzer remains necessary. Such evaluation should quantify measurement error, repeatability, phase-related effects, and uncertainty under resistive, reduced-power-factor, and nonlinear operating conditions.

8. Conclusion

A low-cost dual-node embedded system was developed and experimentally evaluated for the local detection of non-technical losses caused by electrical bypasses in low-voltage service drops. The architecture combines ESP32 microcontrollers, PZEM-004T V3 measurement modules, ESP-NOW communication, synchronized acquisition, and local edge processing without requiring AMI infrastructure, a cellular network, or a local router. The detection model incorporates estimated I^2R technical losses and a current-dependent dynamic threshold. The experimental campaign comprised 40 scenarios, including 20 controlled tests and 20 different residential service drops. Thirty-eight acquisitions satisfied the established synchronization and communication-quality criteria and were used for classification-performance analysis.

The system obtained 9 true positives, 28 true negatives, no false positives, and one false negative, corresponding to an accuracy of 97.37%, sensitivity of 90.00%, specificity of 100.00%, and precision of 100.00%. The false negative occurred in the lowest-power controlled bypass condition of 30 W, identifying a practical sensitivity limit of the evaluated decision criterion.

Technical-loss compensation maintained normal classification in the five QA-valid normal-operation scenarios above 5 kW. In addition, the evaluated transient and nonlinear-load conditions did not produce valid false-positive alerts. The ESP-NOW link achieved an overall packet error rate of 0.79% and a mean transmission latency of 4.36 ms, while timestamp-based acquisition-quality control allowed asynchronous or inadequate measurements to be identified before classification.

The results support the use of the proposed system as a local energy-auditing and bypass-detection tool within the evaluated operating range. Further work should extend the long-duration dataset, evaluate broader conductor and multiphase configurations, perform traceable metrological characterization, assess controlled propagation conditions, and implement cybersecurity mechanisms for the wireless link.

Conflicts of Interest

The authors declare that there are no conflicts of interest regarding the publication of this article.

Funding Statement

The authors received no specific funding for the development of this study.

Acknowledgments

The authors would like to acknowledge the technical support provided in the implementation, installation, and preliminary field evaluation of the prototype.

References

[1] Soma Shekara Sreenadh Reddy Depuru, Lingfeng Wang, and Vijay Devabhaktuni, "Electricity Theft: Overview, Issues, Prevention and a Smart Meter-based Approach to Control Theft," *Energy Policy*, vol. 39, no. 2, pp. 1007-1015, 2011. [CrossRef] [Google Scholar] [Publisher Link]

[2] George M. Messinis, and Nikos D. Hatziargyriou, "Review of Non-Technical Loss Detection Methods," *Electric Power Systems Research*, vol. 158, pp. 250-266, 2018. [CrossRef] [Google Scholar] [Publisher Link]

[3] Paria Jokar, Nasim Arianpoo, and Victor C.M. Leung, "Electricity Theft Detection in AMI using Customers' Consumption Patterns," *IEEE Transactions on Smart Grid*, vol. 7, no. 1, pp. 216-226, 2016. [CrossRef] [Google Scholar] [Publisher Link]

[4] Madalina Mihaela Buzau et al., "Detection of Non-Technical Losses using Smart Meter Data and Supervised Learning," *IEEE Transactions on Smart Grid*, vol. 10, no. 3, pp. 2661-2670, 2019. [CrossRef] [Google Scholar] [Publisher Link]

[5] Esther Villar-Rodriguez et al., "Detection of Non-Technical Losses in Smart Meter Data based on Load Curve Profiling and Time Series Analysis," *Energy*, vol. 137, pp. 118-128, 2017. [CrossRef] [Google Scholar] [Publisher Link]

[6] Zibin Zheng et al., "Wide and Deep Convolutional Neural Networks for Electricity-Theft Detection to Secure Smart Grids," *IEEE Transactions on Industrial Informatics*, vol. 14, no. 4, pp. 1606-1615, 2018. [CrossRef] [Google Scholar] [Publisher Link]

[7] George M. Messinis, Alexandros E. Rigas, and Nikos D. Hatziargyriou, "A Hybrid Method for Non-Technical Loss Detection in Smart Distribution Grids," *IEEE Transactions on Smart Grid*, vol. 10, no. 6, pp. 6080-6091, 2019. [CrossRef] [Google Scholar] [Publisher Link]

[8] Espressif Systems, ESP-NOW, ESP-IDF Programming Guide, 2026. [Online]. Available: https://docs.espressif.com/projects/esp-idf/en/latest/esp32/api-reference/network/esp_now.html

[9] Hooman Firoozi, and Habib Rajabi Mashhadi, "Non-Technical Loss Detection in Limited-Data Low-Voltage Distribution Feeders," *International Journal of Electrical Power and Energy Systems*, vol. 135, pp. 1-18, 2022. [CrossRef] [Google Scholar] [Publisher Link]

[10] Ines Bula et al., "Minimizing Non-Technical Losses with Point-to-Point Measurement of Voltage Drop between 'SMART' Meters," *IFAC-PapersOnLine*, vol. 49, no. 29, pp. 206-211, 2016. [CrossRef] [Google Scholar] [Publisher Link]

[11] Abu Bakr Pengwah, Reza Razzaghi, and Lachlan L.H. Andrew, "Model-Less Non-Technical Loss Detection using Smart Meter Data," *IEEE Transactions on Power Delivery*, vol. 38, no. 5, pp. 3469-3479, 2023. [CrossRef] [Google Scholar] [Publisher Link]

[12] Jin Young Kim et al., "Detection for Non-Technical Loss by Smart Energy Theft with Intermediate Monitor Meter in Smart Grid," *IEEE Access*, vol. 7, pp. 129043-129053, 2019. [CrossRef] [Google Scholar] [Publisher Link]

[13] Ahmed Bin-Halabi, Adnan Nouh, and Mohammad Abouelela, "Remote Detection and Identification of Illegal Consumers in Power Grids," *IEEE Access*, vol. 7, pp. 71529-71540, 2019. [CrossRef] [Google Scholar] [Publisher Link]

[14] Shih-Che Huang, Yuan-Liang Lo, and Chan-Nan Lu, "Non-Technical Loss Detection using State Estimation and Analysis of Variance," *IEEE Transactions on Power Systems*, vol. 28, no. 3, pp. 2959-2966, 2013. [CrossRef] [Google Scholar] [Publisher Link]

[15] Arvind Kumar Gupta, Aurobinda Routray, and V.N. Achutha Naikan, "Detection of Power Theft in Low Voltage Distribution Systems: A Review from the Indian Perspective," *IETE Journal of Research*, vol. 68, no. 6, pp. 4180-4197, 2022. [CrossRef] [Google Scholar] [Publisher Link]

[16] Joaquim L. Viegas et al., "Solutions for Detection of Non-Technical Losses in the Electricity Grid: A Review," *Renewable and Sustainable Energy Reviews*, vol. 80, pp. 1256-1268, 2017. [CrossRef] [Google Scholar] [Publisher Link]

[17] Muhammad Salman Saeed et al., "Detection of Non-Technical Losses in Power Utilities-A Comprehensive Systematic Review," *Energies*, vol. 13, no. 18, pp. 1-25, 2020. [CrossRef] [Google Scholar] [Publisher Link]

[18] Adam Birchfield et al., *Power System Analysis and Design*, 7th ed., Cengage Learning, 2024. [Google Scholar] [Publisher Link]

[19] Charles K. Alexander, and Matthew Sadiku, *Fundamentals of Electric Circuits*, 7th ed., McGraw-Hill Education, 2022. [Google Scholar] [Publisher Link]